Colloid Polym Sci (2009) 287:277–285
DOI 10.1007/s00396-008-1986-8

ORIGINAL CONTRIBUTION

Temperature-programmed synthesis of micron-sized multi-responsive microgels

Zhiyong Meng · Michael H. Smith · L. Andrew Lyon

Received: 15 November 2008 / Revised: 9 December 2008 / Accepted: 10 December 2008 / Published online: 3 January 2009

Abstract A new synthetic protocol for the synthesis of large diameter (2.5 to 5 μm), temperature-, and pH-responsive microgels via aqueous surfactant-free radical precipitation copolymerization is presented. We have found that in this size range, which is not typically attainable using traditional dispersion polymerization approaches, excellent monodispersity and size control are achieved when the synthesis employs a programmed temperature ramp from 45 to 65 °C during the nucleation stage of the polymerization. A combined kinetic and thermodynamic hypothesis for large particle formation under these conditions is described. Particle sizes, volume phase transition temperatures, and pH responsivity were characterized by particle tracking and photon correlation spectroscopy to illustrate their similar behavior to particles made via more traditional routes. These particles have been enabling for various studies in our group where microscopic visualization of the particles is required.

Keywords Temperature-programmed synthesis · Multi-responsive microgels · Micron-size particles · Colloidal crystals · Particle tracking · Photon correlation spectroscopy

Introduction

Microgel particles are spherical polymeric networks swollen by a good solvent and range in size from the submicron to the micron regime [1–7]. There are several microgel compositions that demonstrate stimuli-sensitive behavior, whose physiochemical properties may be affected by temperature [8–11], pH [12–15], ionic strength [16–20], analyte interactions [21–24], and applied external fields [25, 26]. A number of groups have illustrated the potential utility of microgels in rheology modifiers [27, 28], photonic crystals [29–33], wound repair catalysts [34], microlenses [22–24], biosensors [23, 35–37], drug delivery vehicles [21, 38–42], and functional membranes [42, 43]. Commonly, the utility of microgels for a variety of applications depends on controlling the resultant size of the particles while maintaining low size polydispersities. Particle dimensions may also have a role in microgel responsivity since the rate of the volume phase transition increases with decreasing size [44].

Our group has employed surfactant-free precipitation polymerization of thermo/pH responsive materials to produce a variety of monodisperse and responsive particles. For example, 500 nm or smaller diameter microgels were produced by the precipitation polymerization of poly(*N*-isopropylacrylamide-*co*-acrylic acid) (pNIPAm-AAc) at ~70 °C [11]. The addition of increased concentration of an ionic surfactant in the synthetic scheme afforded further reduction of particle size to the sub-100-nm range (i.e., nanogels). These nanogels may enable future drug delivery applications since materials of this size regime can be transported through the cell membrane via endocytosis, for example. Furthermore, bioconjugation of the nanogels may allow additional functionality at the biological interface [45]. In addition to drug delivery vehicles, our group has developed microlenses for biosensing [23, 24] and has also fabricated colloidal crystals composed of responsive microgels [29, 33]. Optical microscopy has been employed to assess microgel behavior in these studies, as investigations

Z. Meng · M. H. Smith · L. A. Lyon (✉)
School of Chemistry and Biochemistry & Petit Institute for Bioengineering and Bioscience,
Georgia Institute of Technology,
Atlanta, GA 30332-0400, USA
e-mail: lyon@gatech.edu

of microlens response or colloidal crystal structure benefit tremendously from direct inspection of the particles [23, 46, 47]. To enable such studies, larger particles than those attainable via typical dispersion polymerization approaches (e.g., sizes >2.5 μm in diameter) were required. In addition, it was important that the range of temperature- and pH-responsive polymers typically used was conserved in this approach.

In this investigation, we describe the aqueous synthesis of large (2.5 to 5 μm), multi-responsive, monodisperse microgel particles composed of *N*-isopropylacrylamide (NIPAm) or *N*-isopropylmethacrylamide (NIPMAm) and acrylic acid (AAc) via temperature-ramp surfactant-free radical precipitation polymerization. This approach affords particles with properties that have been ideal for our microlensing and crystallization studies, suggesting that they may be useful for other applications where many-micron colloidal particles would be preferred over submicron-sized counterparts.

Experimental

Materials The monomers NIPAm (TCI) and NIPMAm (Aldrich) were purified by recrystallization from *n*-hexane (J. T. Baker). AAc (Fluka), *N*,*N*'-methylene (bisacrylamide) (BIS, Aldrich) and ammonium persulfate (APS, Aldrich) were used as received. Water for polymerizations, purification, and dispersion preparations was distilled, deionized to a resistance of 18 MΩ·cm (Barnstead E-Pure system), and filtered through a 0.2-μm filter to remove particulate matter.

Synthesis of large microgel particles Microgels composed of p(NIPAm-*co*-AAc) or p(NIPMAm-*co*-AAc) with a size above 2.5 μm were synthesized via temperature-ramp, surfactant-free, radical precipitation polymerization. In a typical synthesis, the monomers NIPAm (1.8 g) and AAc (0.2 g) and the cross-linker BIS (0.06 g) were dissolved in 100 mL of distilled, deionized water and filtered through a 0.2-μm filter to remove particulate matter. Deionized water (25 mL) was used to transfer and wash throughout filtration. After delivering the monomer solution to a 250 mL three-neck round-bottom flask via a 20-mL syringe with a 0.2-μm in-line filter, the flask was equipped with a thermometer, condenser/N_2 outlet, stir bar, and a N_2 inlet. The reaction system was purged with N_2 for 1 h while equilibrating to a temperature of 45 °C. The monomer solution (125-mL volume) was then maintained at 45 °C for 15 min at a stir rate of 450 rpm. A 5-mL aliquot of a 0.078 M aqueous solution of the initiator APS was delivered to the monomer solution via a 5-mL syringe with a 0.2-μm inline filter to initiate the polymerization. Immediately following initiation, a temperature ramp from 45 to 65 °C was applied to the solution at a ramp rate of 30 °C/h. Following completion of the ramp, the polymerization was allowed to proceed overnight at 65 °C. After polymerization, the resulting turbid reaction product was filtered through glass wool to remove a small amount of coagulum [2].

Microgel particle purification Microgels were purified by centrifugation to separate unreacted monomers, oligomers, and initiator from the microgels. The synthesis product was separated at a relative centrifugal force of 15,422×*g* for 1 h, followed by removal of the supernatant and re-dispersion of microgel pellets by shaking with fresh deionized water. The centrifugation and re-dispersion process was repeated four times. After purification, the microgel dispersion was lyophilized at −42 °C under 40×10^{-3} mbar for 48–72 h. The freeze-dried product was a hygroscopic white powder.

Photon correlation spectroscopy Temperature-programmed photon correlation spectroscopy (PCS; Protein Solutions, Inc.) was used to determine the mean particle sizes and particle size distributions for 0.01 wt.% of microgel particles in pH 3.0 aqueous buffer using a laser with wavelength of 690 nm. This technique has been applied extensively to the characterization of microgel particles, as it allows for in situ size characterization of soft or solvent swollen particles that cannot be reliably characterized by electron microscopy due to deformation and/or dehydration under vacuum [11]. The dispersed particles in water were allowed to equilibrate thermally for 60 min before measurements were taken at each temperature. In the data presented below, each data point at a given temperature represents the average value of 20 measurements, with a 10-s integration time for each measurement. Hydrodynamic radii of the particles were calculated from diffusion coefficients using the Stokes–Einstein equation. All correlogram analyses were performed using manufacturer-supplied software (Dynamics v.5.25.44, Protein Solutions, Inc.). The intensity–intensity autocorrelation function $G^{(2)}(q,t)$ in the self-beating mode was measured with a Protein Solutions DynaPro 256-channel digital correlator.

$$G^{(2)}(q,t) = A\left[1 + B\left|g^{(1)}(q,t)\right|^2\right] \quad (1)$$

where $q=(4\pi n/\lambda_0)\sin(\theta/2)$ with n, λ_0, and θ being the solvent refractive index, the wavelength of light in vacuo, and the scattering angle, respectively; t is the delay time, A the measured baseline, B the coherence factor, and $g^{(1)}(q,t)$ the normalized electric field time correlation function. With Laplace inversion of $g^{(1)}(q,t)$, the translational diffusion coefficient, D, and its distribution could be obtained. The hydrodynamic diameter can then be deduced from Stokes–Einstein equation (*vide infra*). Note that the upper limit of

particle diameter for PCS measurement is about 2.5 μm; particles with diameter larger than 2.5 μm do not give an autocorrelation function that can be statistically correlated with the diffusion coefficient. This is largely due to the low number density of particles in the scattering volume, which results in a significant contribution to the scattering signal from number density fluctuations [2, 48].

Preparation of microgel dispersions Aqueous buffers were prepared using recipes from buffer calculator developed by R. Beynon at the University of Liverpool [49]. The microgel dispersions were prepared by first dispersing approximately 10 mg pNIPAm-AAc powder in 10 g of distilled, deionized water and shaking for 1 week to obtain a 0.1-wt.% dispersion. A 250-μL aliquot of the 0.1-wt.% dispersion was then diluted to a concentration of 0.01 wt.% in aqueous buffer. The pH values with errors were measured to ±0.1 units with a pH meter (pH 430, Corning Corp.) with an Accumet probe (Cole-Palmer). The ionic strength was controlled by adding the appropriate amount of NaCl, as determined from the buffer calculation. Because ionic strength is proportional to the conductivity, the ionic strength of pH buffers was determined by measuring the conductivity of corresponding pH buffers. The conductivity was measured with a Pinnacle 541 conductivity meter (Corning Corp.) with a "3 in 1" Combo w/RJ probe (Corning Corp.). Conductivity values for all aqueous buffers were 1.48±0.20 mS/cm. For microsopic visualization, the dilute dispersions were introduced into 5.0×2.0×0.1 mm Vitrotube™ rectangular capillaries (Fiber Optic Center, Inc.) by capillary force at room temperature and then sealed with Epoxy Putty™ (ITW Devcon®) resin.

Tracking particles by video microscopy Brightfield images (transmission mode) were obtained with an inverted Olympus IX-71 microscope equipped with a ×100 oil immersion objective and Andor™ LUCA electron multiplying charge-coupled device camera. The sample temperature was controlled with a temperature stage (Physitemp) as well as an objective heater (Bioptechs) to within ±0.1 °C. Typically, after thermal equilibration for 60 min, the images were recorded at the middle layer of microgel assemblies, ~50 μm away from both upper and lower walls to minimize perturbations from the glass surface. Andor™ iQ 3.0 software were used to monitor and record the motion of microgels at a recording rate of 30 frames/s. To enable quantification of particle motion, the microgel positions in an image time series acquired via video microscopy [46] were analyzed using a modified version of the particle tracking code originally developed by Crocker and Grier [50] in the IDL 6.0 (Research System, Inc.) programming environment, as described previously [33, 51]. A particularly illustrative means for presenting the dynamics of microgel particles in those phases is through a double logarithm plot of the microgel mean squared displacement (MSD) vs. lag time (τ). The MSD of colloidal particles in an ensemble is given by

$$\mathrm{MSD}(\tau) = \left\langle [r_i(t+\tau) - r_i(t)]^2 \right\rangle_{i,t} \tag{2}$$

where $r_i(t)$ is the position vector of the ith particle at time t, τ is the lag time, and $\langle\rangle_{i,t}$ indicates the spatial average over the ensemble of particles as well as all starting times t. In the colloidal gas regime, where particle motion is purely diffusive and interactions between particles are minimal, the MSD should be proportional to lag time

$$\mathrm{MSD}(\tau) = 2dD\tau \tag{3}$$

where d is the dimensionality of the displacement vectors and D is the translational self-diffusion coefficient of microgel particles. Very dilute (0.01 wt.%) microgel suspensions were tracked by video microscopy to obtain linear MSD vs. τ plots; because dilute dispersion exhibit unhindered diffusion, the translational self-diffusion coefficient D could be extracted from the slope of this plot by using Eq. 4.

$$D = \frac{d\mathrm{MSD}(\tau)}{d\tau} \Big/ 2d \tag{4}$$

Combining this with the Stokes–Einstein equation,

$$D = \frac{k_\mathrm{B}T}{d\pi\sigma\eta_S} \tag{5}$$

yields an expression from which the hydrodynamic diameter (σ) in the dilute regime can be obtained

$$\sigma = \frac{2k_\mathrm{B}T}{\pi\eta_\mathrm{S}\frac{d\mathrm{MSD}(\tau)}{d\tau}} \tag{6}$$

where k_B is Boltzmann constant, T absolute temperature, $\frac{d\mathrm{MSD}(\tau)}{d\tau}$ the slope of the linear MSD vs. τ plot, and η_s the intrinsic viscosity of solvent.

Fluorometry The volume phase transition temperature (VPTT) value for both pNIPAm-AAc and pNIPMAm-AAc microgels was measured from turbidity curves collected on a steady-state fluorescence spectrophotometer (Photon Technology International), equipped with a Model 814 PMT photon-counting detector. All turbidity experiments were performed at pH 3.0 (10 mM ionic strength). Scattering was measured at 600 nm, and a temperature ramp was typically set from 25 °C to a maximum of 50 °C for all measurements. A ramp rate of 0.25 °C/min was used, data were collected with an integration time of 1 s per point.

Results and discussion

The hydrodynamic diameter calculation of large microgel particles is described above. Generally, the large microgel particles are colloidally stable in a buffer over a wide pH range due to the electrosteric interactions between particles [52], even though they are fairly sticky to glass surfaces, presumably due to hydrogen bonding interactions [33]. In the particle tracking approach, digital video microscopy was used to obtain a series of images with temporal and spatial information of microgel particles diffusing in the focus plane. To balance the irreversible attachment of some particles on the inner wall of borosilicate rectangular capillaries with the thermal equilibrium of particles in the bulk dispersions [33], images were acquired 30 min after sample preparation. Figure 1a and c shows the microscopy images and trajectories of large pNIPAm-AAc and pNIPMAm-AAc microgel particles (0.01 wt.% polymer in pH 3.5 buffer, ionic strength of 10 mM), where bright particles (circled) are within the focal plane. Figure 1b and d shows the trajectories of pNIPAm-AAc and pNIPMAm-AAc particles, respectively, obtained by quantitative image analysis of movies taken by video optical microscopy [50]. The mismatch between particle trajectories and the microscope images is attributed to the motion of some particles in and out of the focal plane over the course of the measurement. The trajectories of these particles are purely diffusive, and no interaction between particles is observed in these dilute microgel dispersions. The particle sizes can be extracted by the particle-tracking algorithm combined with Stokes–Einstein equation shown above, which gives a hydrodynamic diameter of approximately 3.0±0.2 μm for pNIPAm-AAc microgels and 2.6±0.2 μm for pNIPMAm-AAc microgels, respectively (in pH 3.5 buffer at 20.0 °C) ,whereas PCS does not give a reasonable measurement of particle size for such large microgel particles.

Figure 2a shows the change of average particle size vs. pH. Our characterization utilized particle tracking routines for in situ determination of the hydrodynamic diameters of larger microgel particles in aqueous buffer. It was not possible to determine pH responsivity by PCS since particle number densities within the scattering volume change drastically for such large sizes at 20 °C. As a result, the scattering intensities by PCS do not statistically correlate with the diffusion coefficients and hydrodynamic diameters of particles could not be determined. A notable exception was for measurements made at pH 3.0. In pH 3.0 buffer at 20 °C, tracking algorithms resulted in a calculated hydrodynamic diameter of approximately 2.7±0.2 μm, slightly larger than particle size measured by PCS, 2.5± 0.2 μm. The error bars in Fig. 2a represent the measured polydispersity, which is below 10%. Furthermore, particle diameters increase from 2.7 μm at pH 3.0 to 4.4 μm at pH 6.0, representing a volume increase of >4-fold through-

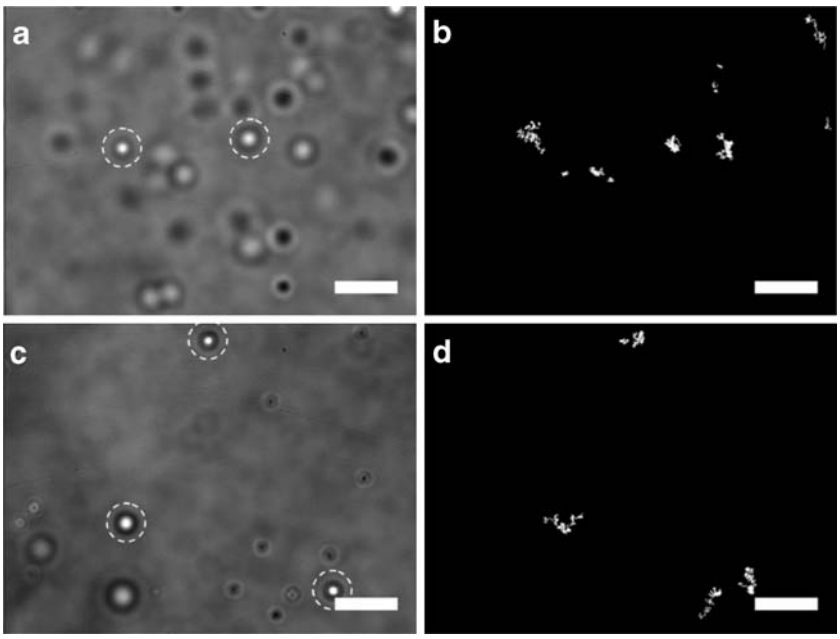

Fig. 1 Digital microscopy images and particle trajectories for pNIPAm-AAc and pNIPMAm-AAc microgel particles (both at 0.01 wt.% polymer in pH 3.5 buffer). The microscopy image and particle trajectories for pNIPAm-AAc particles are displayed in **a** and **b**, respectively. The microscopy image and particle trajectories for pNIPMAm-AAc particles are displayed in **c** and **d**, respectively. The particles on the focus plane of microscope are *circled by dashed lines*. Note that particles moving out of the focal plane are excluded from analysis with IDL routines by setting the brightness threshold. The sizes of pNIPAm-AAc and pNIPMAm-AAc particles are approximately 3.0±0.2 and 2.6±0.2 μm, respectively, based upon particle tracking and the Stokes–Einstein equation. Scale bar=10 μm

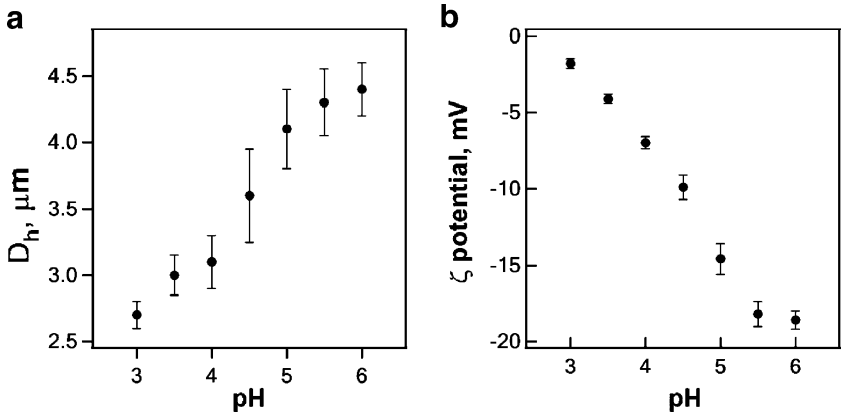

Fig. 2 **a** The hydrodynamic diameter (D_h) and **b** ζ potential vs. pH for pNIPAm-AAc microgels. The polydispersities of the hydrodynamic diameters are shown as error bars, with the size polydispersities being approximately 10%. Note that the average particle size increases drastically at a pH close to the pK_a value of the AAc monomer (pK_a=4.25), whereas the ζ potential becomes more negative as the pH traverses the pK_a

out the pH ramp. The pH-responsive swelling behavior is due to the deprotonation of AAc segments at higher pH values, which leads to the increase of electrostatic repulsion between carboxylate anions and the increase of osmotic pressure inside microgel particles, thereby swelling the polymeric networks [53–55]. In addition, the zeta-potential of the pNIPAm-AAc microgel particles over the pH range from 3.0 to 6.0 is presented in Fig. 2b, which confirms the pH responsivity of large particles [56, 57]. Note that pNIPAm-AAc microgel particles with diameters below 1 μm display a similar pH responsivity to those observed in this study [55, 58, 59].

Figure 3 shows the temperature-responsivity of pNIPAm-AAc microgel particles in pH 3.0 buffer [11, 59]. Because the particle size in this case is below 2.5 μm, we found that PCS could reliably be used to determine the in situ size of microgel particles from 20 to 40 °C [33]. The error bars represent the polydispersities, which again are below 10%. The VPTT of pNIPAm-AAc microgels is approximately 30 °C, at which the size of particles decreased from 2.2 μm down to approximately 1.2 μm, corresponding to the well-known volume phase transition of pNIPAm [44]. The volume change associated with the VPT is ~8-fold, which is similar to the volume change for smaller particles of similar composition [60]. However, the VPTT of these large pNIPAm-AAc microgel particles is slightly lower than that of smaller pNIPAm-AAc microgels (31 °C) synthesized previously in our group [29, 33, 51, 61]. This is likely due to the fact that the particles described in this are ~15 mol% AAc as opposed to the 10 mol% particles synthesized previously; it is known that with increasing AAc content in copolymer, the VPTT of pNIPAm-AAc microgels decreases [55]. It should be noted, however, that AAc incorporation is not required to obtain these particle sizes. It is included in this study at these concentrations because it is needed for a variety of microlens and crystallization studies ongoing in our group.

In addition to these applications, our group has expressed interest in large, monodisperse particles that are compatible at the biological interface. Such materials would ideally remain swollen under in vivo conditions, at temperatures significantly higher than the VPTT of NIPAm-based microgels (i.e., >37 °C). By employing NIPMAm monomer in our precipitation polymerization, microgels were produced of similar size as pNIPAm-AAc particles (Fig. 1). However, the thermal responsivities of these materials are fundamentally different, where NIPMAm-based microgels traditionally demonstrate a VPTT above 37 °C [62]. To compare the VPTT behavior between both particle types, turbidity curves were collected for particles by steady-state fluorescence spectrophotometry (Fig. 4). The pNIPAm-AAc microgels show a distinct phase transition at ~30 °C (Fig. 4a), which is in agreement with photon correlation data (Fig. 3). The characterized VPTT of the pNIPMAm-AAc particles is considerably higher, demonstrating a broad phase transition at ~35 °C (Fig. 4b). Similar to the NIPAm particles, this VPTT is lower than that observed for

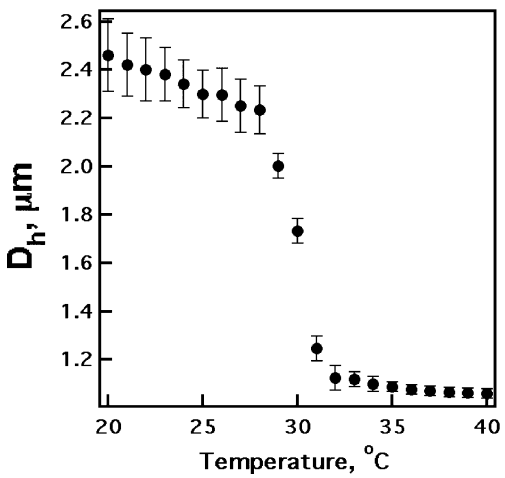

Fig. 3 The temperature hydrodynamic diameter of pNIPAm-AAc microgels in pH 3.0 buffer. The hydrodynamic diameter was measured by PCS with a programmed temperature ramp from 20 to 40 °C. The error bars represent the size polydispersities, which are below 10%. Note that the VPTT of microgel particles is approximately 30 °C, as described in the literature for similar polymer compositions [1, 82]

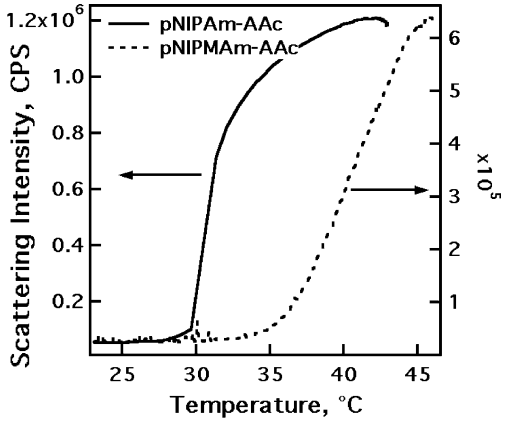

Fig. 4 Temperature-dependant turbidity measurements for large pNIPAm-AAc and pNIPMAm-AAc particles in pH 3.0 buffer. A phase transition is observed for pNIPAm-AAc microgels at ~30 °C, in agreement with photon correlation data (see Fig. 3). A shift in the VPTT for pNIPMAm-AAc particles to ~35 °C and a broadening of the phase transition is observed, which is in agreement with small particle formulations using NIPMAm as a monomer [62–64]

previously produced particles, which contain less AAc incorporation [11, 63, 64]. Although the phase transition for this NIPMAm-AAc particle formulation is below 37 °C, the VPTT may be elevated by decreasing AAc copolymerization. It is notable that our pNIPAm-AAc and pNIPMAm-AAc microgels were synthesized under identical total monomer/cross-linker concentrations with the same temperature ramp precipitation polymerization method. These data demonstrate that within this narrow range of VPTTs, this temperature ramp approach is not limited to pNIPAm-based copolymers. However, it is currently unknown whether polymers with lower critical solution temperature (LCST) values above the initiation temperature (45 °C) can be employed in this temperature-ramp precipitation polymerization approach. Our group is currently investigating this synthetic scheme as a springboard to produce multiple types of large microgel materials of varying responsivity.

Owing to their excellent monodispersity, these particles also self-assemble into colloidal crystals [10, 47, 65–70]. The transmission-mode microscopy image and trajectories of colloidal crystals assembled from a 2.0 wt.% dispersion of pNIPAm-AAc microgels in pH 3.0 buffer is shown in Fig. 5. The left panel is the microscopic image of the middle layer of colloidal crystals of microgel particles. The right panel includes the trajectories of microgel particles in the focus plane. Based upon the particle positions in microscopic image series, the radial distribution function could be obtained. The first peak of radial distribution function vs. center-to-center distance corresponds to the in situ average diameter of particles in colloidal crystals [71]. The particle size calculated from Fig. 5, 2.8±0.1 μm, is smaller than that calculated from the data in Fig. 1, 3.0± 0.2 μm, due to an osmotic deswelling effect observed previously in such colloidal assemblies [72]. The above results suggest that the larger pNIPAm-AAc microgel particles show similar crystallization behavior to their smaller counterparts, which have been reported previously [33, 47, 60, 70].

Particle formation

Whereas we have not, to this point, undertaken a detailed mechanistic study of this synthetic approach, there are a number of conclusions that can be drawn from these data and from previous polymerization studies. Generally, the temperature used for pNIPAm- or pNIPMAm-based microgel particle synthesis is ~70 °C, where resulting particle size characterizations reveal hydrodynamic diameters of 800 nm or smaller in pH 3.0 buffer [1, 11, 58, 73]. The size of microgel particles by this scheme may be further influenced by changing a variety of reaction conditions, including the solvent composition [73], monomer/comonomer concentration [74], and degree of cross-linking [73, 75–77]. We have shown that precipitation polymerization reactions at lower temperatures (such as 60 °C) results in an increase in particle size up to 1.5 μm in pH 3.0 buffer [33]. However, when we decreased the reaction temperature further (e.g., to 50 °C), an excessive amount of coagulum formed instead of a monodisperse colloid [78]. It was clear, given the phase separating nature of the reaction, that temperature plays a critical role in the control of particle size if other parameters of polymerization, such as monomer concentration, comonomer/monomer ratio,

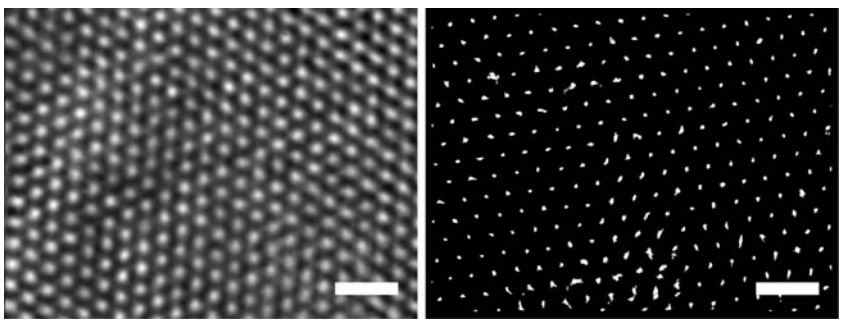

Fig. 5 A digital microscopy image and particle trajectories for pNIPAm-AAc microgels assembled into colloidal crystals (2.0±0.1 wt.% in pH 3.5 buffer). Note that the size of the particles as determined from radial distribution analyses is smaller than 3.0 μm, probably due to an osmotic deswelling effect observed previously [72]. Scale bar=10 μm

cross-linker/monomer ratio, and initiator/monomer ratio, stirring speed, degas time, and flow rate of N_2 are fixed. To obtain monodisperse microgel particles with diameters larger than 2.5 μm, we needed a new strategy for the precipitation polymerization.

Under the described synthetic conditions (when reaction temperatures reach 45 °C) persulfate anions decompose to form primary radicals [79], which subsequently attack monomers to form oligomeric radical chains (<3 monomer units). When the oligomeric radical chains reach a critical length (>5 monomer units) at a temperature higher than the LCST of pNIPAm-AAc segments (30 °C in this study), they collapse to form thermodynamically unstable nuclei with a radical trapped in or on their surface for further reaction [80]. This stage is known as nucleation, forming a population of collapsed precursor particles. Because the decomposition rate of initiator is decreased at lower temperatures [79], reaction temperatures below conventional initiation temperatures (<60–70 °C) may reduce the oligomeric radical concentration, thereby lowering the abundance of collapsed nuclei. This lower nuclei concentration likely favors particle growth mechanisms that do not involve appreciable nuclei aggregation due to the relatively low possibility for bimolecular termination of two radicals on different nuclei. Furthermore, immediately after initiation, the monomer concentration in the reaction mixture is higher than later stages. The lower nuclei concentration combined with higher monomer concentration at initial reaction times ensures a higher propagation rate than initiation rate, which favors the growth of nuclei with similar speed in early polymerization stages [80]. As the reaction proceeds and monomer is consumed, the monomer concentration decreases, thereby decreasing the propagation rate. To compensate for this decrease in propagation rate (due to monomer consumption), the reaction temperature is ramped up from 45 to 65 °C. This ramp increases the propagation rate constant and also results in the increased decomposition of persulfate, thereby generating more radicals.

After approximately 40 min of polymerization, the temperature ramp is completed at 65 °C, and the majority of monomers were likely converted to oligomeric radicals, nuclei, and precursor particles [59]. Therefore, the nucleation stage is replaced by the growth of the nuclei/particles via monomer addition, nuclei absorption, and nuclei aggregation [59, 74]. At this elevated temperature (65 °C), growth on the nuclei/precursor particles becomes more favorable than nucleation due to much lower monomer concentration and stronger van der Waals attraction between nuclei and/or precursor radicals than nucleation stage. Because of the electrostatic repulsive interactions arising from the sulfate end groups, microgel particles are stabilized from coagulation while still capturing oligomeric radicals and unstable nuclei, thereby precluding any secondary nucleation from unstable nuclei [81].

Conclusions

By introducing a temperature ramp in the early stage of the surfactant-free radical precipitation polymerization, the mean size of the resultant multi-responsive microgel particles has been increased significantly while maintaining a low polydispersity (≤10%). The larger microgel particles demonstrate similar thermal and pH responsivity to their smaller counterparts of similar composition. We have demonstrated that the mean diameter of pNIPAm-AAc microgel particles can swell from 2.5 to 4.5 μm by increasing the pH. Furthermore, we have shown that the synthetic protocol could be extended from NIPAm to NIPMAm for the preparation of larger particles with similar sizes resulting from similar reaction conditions. This synthetic scheme may be promising for producing other monodisperse, thermoresponsive microgel particles for applications as microlenses, biosensors, and drug delivery vehicles.

Acknowledgment This manuscript is dedicated to Professor Haruma Kawaguchi on the occasion of his retirement from Keio University. LAL acknowledges funding from the Georgia Institute of Technology and the Centers for Disease Control.

References

1. Pelton RH, Chibante P (1986) Preparation of aqueous latices with N-isopropylacrylamide. Colloids Surf 20:247–256
2. Murray MJ, Snowden MJ (1995) The preparation, characterization and applications of colloidal microgels. Adv Colloid Interface Sci 54:73–91
3. Pelton R (2000) Temperature-sensitive aqueous microgels. Adv Colloid Interface Sci 85:1–33
4. Staudinger H, Husemann E (1935) Über hochpolymere Verbindungen, 116. Mitteil.: Über das begrenzt quellbare Poly-styrol. Ber Chem 68:1618–1634
5. Medalia AI (1951) Structure and thermodynamics of elastomeric microgel. J Polym Sci 6:423–431
6. Shashoua VE, Beaman RG (1958) Microgel—an idealized polymer molecule. J Polym Sci 33:101–117
7. Sieglaff CL (1963) Viscosity and swelling behaviour of lightly crosslinked microgels. Polymer 4:281–284
8. Keerl M, Richtering W (2007) Synergistic depression of volume phase transition temperature in copolymer microgels. Colloid Polym Sci 285:471–474
9. Duracher D, Elaissari A, Pichot C (1999) Characterization of cross-linked poly(N-isopropylmethacrylamide) microgel latexes. Colloid Polym Sci 277:905–913
10. Senff H, Richtering W (1999) Temperature sensitive microgel suspensions: colloidal phase behavior and rheology of soft spheres. J Chem Phys 111:1705–1711

11. Jones CD, Lyon LA (2000) Synthesis and characterization of multiresponsive core-shell microgels. Macromolecules 33:8301–8306
12. Ni H, Kawaguchi H, Endo T (2007) Preparation of pH-sensitive hydrogel microspheres of poly(acrylamide-co-methacrylic acid) with sharp pH-volume transition. Colloid Polym Sci 285:819–826
13. Ni HM, Kawaguchi H, Endo T (2007) Characteristics of pH-sensitive hydrogel microsphere of poly(acrylamide-co-meth acrylic acid) with sharp pH-volume transition. Colloid Polym Sci 285:873–879
14. Dai S, Ravi P, Tam KC (2008) pH-Responsive polymers: synthesis, properties and applications. Soft Matter 4:435–449
15. Tan BH, Tam KC (2008) Review on the dynamics and microstructure of pH-responsive nano-colloidal systems. Adv Colloid Interface Sci 136:25–44
16. Greinert N, Richtering W (2004) Influence of polyelectrolyte multilayer adsorption on the temperature sensitivity of poly(N-isopropylacrylamide) (PNiPAM) microgels. Colloid Polym Sci 282:1146–1149
17. Kim JH, Ballauff M (1999) The volume transition in thermosensitive core-shell latex particles containing charged groups. Colloid Polym Sci 277:1210–1214
18. Kashiwabara M, Fujimoto K, Kawaguchi H (1995) Preparation of monodisperse, reactive hydrogel microspheres and their amphoterization. Colloid Polym Sci 273:339–345
19. Daly E, Saunders BR (2000) A study of the effect of electrolyte on the swelling and stability of poly(N-isopropylacrylamide) microgel dispersions. Langmuir 16:5546–5552
20. Zha LS, Hu JH, Wang CC, Fu SK, Luo MF (2002) The effect of electrolyte on the colloidal properties of poly(N-isopropylacrylamide-co-dimethylaminoethylmethacrylate) microgel latexes. Colloid Polym Sci 280:1116–1121
21. Nayak S, Lee H, Chmielewski J, Lyon LA (2004) Folate-mediated cell targeting and cytotoxicity using thermoresponsive microgels. J Am Chem Soc 126:10258–10259
22. Serpe MJ, Kim J, Lyon LA (2004) Colloidal hydrogel microlenses. Adv Mater 16:184–187
23. Kim J, Nayak S, Lyon LA (2005) Bioresponsive hydrogel microlenses. J Am Chem Soc 127:9588–9592
24. Kim JS, Singh N, Lyon LA (2006) Label-free biosensing with hydrogel microlenses. Angew Chem Int Ed 45:1446–1449
25. Bhattacharya S, Eckert F, Boyko V, Pich A (2007) Temperature-, pH-, and magnetic-field-sensitive hybrid microgels. Small 3:650–657
26. Snoswell DRE, Brill RK, Vincent B (2007) pH-Responsive microrods produced by electric-field-induced aggregation of colloidal particles. Adv Mater 19:1523–1527
27. Senff H, Richtering W (2000) Influence of cross-link density on rheological properties of temperature-sensitive microgel suspensions. Colloid Polym Sci 278:830–840
28. Wolfe MS (1992) Dispersion and solution rheology control with swellable microgels. Prog Org Coat 20:487–500
29. Lyon LA, Debord JD, Debord SB, Jones CD, McGrath JG, Serpe MJ (2004) Microgel colloidal crystals. J Phys Chem B 108:19099–19108
30. Suzuki D, McGrath JG, Kawaguchi H, Lyon LA (2007) Colloidal crystals of thermosensitive, core/shell hybrid microgels. J Phys Chem C 111:5667–5672
31. Reese CE, Mikhonin AV, Kamenjicki M, Tikhonov A, Asher SA (2004) Nanogel nanosecond photonic crystal optical switching. J Am Chem Soc 126:1493–1496
32. Xu SQ, Zhang JG, Paquet C, Lin YK, Kumacheva E (2003) From hybrid microgels to photonic crystals. Adv Funct Mater 13:468–472
33. Meng Z, Cho JK, Debord S, Breedveld V, Lyon LA (2007) Crystallization behavior of soft, attractive microgels. J Phys Chem B 111:6992–6997
34. Freemont TJ, Saunders BR (2008) PH-responsive microgel dispersions for repairing damaged load-bearing soft tissue. Soft Matter 4:919–924
35. Retama JR, Lopez-Ruiz B, Lopez-Cabarcos E (2003) Microstructural modifications induced by the entrapped glucose oxidase in cross-linked polyacrylamide microgels used as glucose sensors. Biomaterials 24:2965–2973
36. Khoury C, Adalsteinsson T, Johnson B, Crone WC, Beebe DJ (2003) Tunable microfabricated hydrogels - A study in protein interaction and diffusion. Biomed Microdevices 5:35–45
37. Perez JPH, Lopez MSP, Lopez-Cabarcos E, Lopez-Ruiz B (2006) Amperometric tyrosinase biosensor based on polyacrylamide microgels. Biosens Bioelect 22:429–439
38. Kawaguchi H, Fujimoto K, Mizuhara Y (1992) Hydrogel microspheres.3. Temperature-dependent adsorption of proteins on poly-N-isopropylacrylamide hydrogel microspheres. Colloid Polym Sci 270:53–57
39. Fang SJ, Kawaguchi H (2002) A thermosensitive amphoteric microsphere and its potential application as a biological carrier. Colloid Polym Sci 280:984–989
40. Kiser PF, Wilson G, Needham D (2000) Lipid-coated microgels for the triggered release of doxorubicin. J Control Release 68:9–22
41. Nolan CM, Gelbaum LT, Lyon LA (2006) H-1 NMR investigation of thermally triggered insulin release from poly(N-isopropylacrylamide) microgels. Biomacromolecules 7:2918–2922
42. Serpe MJ, Yarmey KA, Nolan CM, Lyon LA (2005) Doxorubicin uptake and release from microgel thin films. Biomacromolecules 6:408–413
43. Ogawa K, Wang B, Kokufuta E (2001) Enzyme-regulated microgel collapse for controlled membrane permeability. Langmuir 17:4704–4707
44. Hirose Y, Amiya T, Hirokawa Y, Tanaka T (1987) Phase-transition of submicron gel beads. Macromolecules 20:1342–1344
45. Blackburn WH, Lyon LA (2008) Size-controlled synthesis of monodisperse core/shell nanogels. Colloid Polym Sci 286:563–569
46. Murray CA, Grier DG (1996) Video microscopy of monodisperse colloidal systems. Annu Rev Phys Chem 47:421–462
47. Hellweg T, Dewhurst CD, Bruckner E, Kratz K, Eimer W (2000) Colloidal crystals made of poly(N-isopropylacrylamide) microgel particles. Colloid Polym Sci 278:972–978
48. Pecora R (1985) Dynamic light scattering. Plenum, New York
49. Beynon R (2006) Buffer calculator. http://www.liv.ac.uk/buffers
50. Crocker JC, Grier DG (1996) Methods of digital video microscopy for colloidal studies. J Colloid Interface Sci 179:298–310
51. St. John AN, Breedveld V, Lyon LA (2007) Phase behavior in highly concentrated assemblies of microgels with soft repulsive interaction potentials. J Phys Chem B 111:7796–7801
52. Fritz G, Schadler V, Willenbacher N, Wagner NJ (2002) Electrosteric stabilization of colloidal dispersions. Langmuir 18:6381–6390
53. Dai S, Ravi P, Tam KC (2008) pH-Responsive polymers: synthesis, properties, and applications. Soft Matter 4:435–449
54. Tan BH, Tam KC (2008) Review on the dynamics and microstructure of pH-responsive nano-colloidal systems. Adv Colloid Interface Sci 136:25–44
55. Kratz K, Hellweg T, Eimer W (2000) Influence of charge density on the swelling of colloidal poly(N-isopropylacrylamide-co-acrylic acid) microgels. Colloid Surf A-Physicochem Eng Asp 170:137–149
56. Rasmusson M, Vincent B, Marston N (2000) The electrophoresis of poly(N-isopropylacrylamide) microgel particles. Colloid Polym Sci 278:253–258
57. Ohshima H (2007) Electrokinetics of soft particles. Colloid Polym Sci 285:1411–1421

58. Snowden MJ, Chowdhry BZ, Vincent B, Morris GE (1996) Colloidal copolymer microgels of N-isopropylacrylamide and acrylic acid: pH, ionic strength and temperature effects. J Chem Soc-Faraday Trans 92:5013–5016
59. Zhou SQ, Chu B (1998) Synthesis and volume phase transition of poly(methacrylic acid-co-N-isopropylacrylamide) microgel particles in water. J Phys Chem B 102:1364–1371
60. Debord SB, Lyon LA (2003) Influence of particle volume fraction on packing in responsive hydrogel colloidal crystals. J Phys Chem B 107:2927–2932
61. Serpe MJ, Lyon LA (2004) Optical and acoustic studies of pH-dependent swelling in microgel thin films. Chem Mat 16:4373–4380
62. Tang YC, Ding YW, Zhang GZ (2008) Role of methyl in the phase transition of poly(N-isopropylmethacrylamide). J Phys Chem B 112:8447–8451
63. Blackburn WH, Lyon LA (2008) Size-controlled synthesis of monodisperse core/shell nanogels. Colloid Polym Sci 286:563–569
64. Duracher D, Elaissari A, Pichot C (1999) Preparation of poly(N-isopropylmethacrylamide) latexes kinetic studies and characterization. J Polym Sci Pol Chem 37:1823–1837
65. Debord SB, Lyon LA (2003) Influence of particle volume fraction on packing in responsive hydrogel colloidal crystals. J Phys Chem B 107:2927–2932
66. St. John AN, Breedveld V, Lyon LA (2007) Phase behavior in highly concentrated assemblies of microgels with soft repulsive interaction potentials. J Phys Chem B 111:7796–7801
67. Meng Z, Cho JK, Debord S, Breedveld V, Lyon LA (2007) Crystallization behavior of soft, attractive microgels. J Phys Chem B 111:6992–6997
68. Xu SQ, Zhang JG, Paquet C, Lin YK, Kumacheva E (2003) From hybrid microgels to photonic crystals. Adv Funct Mater 13:468–472
69. Suzuki D, McGrath JG, Kawaguchi H, Lyon LA (2007) Colloidal crystals of thermosensitive, core/shell hybrid microgels. J Phys Chem C 111:5667–5672
70. Lyon LA, Debord JD, Debord SB, Jones CD, McGrath JG, Serpe MJ (2004) Microgel colloidal crystals. J Phys Chem B 108:19099–19108
71. Hansen JP, McDonald IR (2006) Theory of simple liquids. Elsevier, Amsterdam
72. Tan BH, Tam KC, Lam YC, Tan CB (2005) Osmotic compressibility of soft colloidal systems. Langmuir 21:4283–4290
73. Kawaguchi H, Kawahara M, Yaguchi N, Hoshino F, Ohtsuka Y (1988) Hydrogel microspheres.1. Preparation of monodisperse hydrogel microspheres of sub-micron or micron size. Polym J 20:903–909
74. Kawaguchi H, Yamada Y, Kataoka S, Morita Y, Ohtsuka Y (1991) Hydrogel microspheres. 2. Precipitation copolymerization of acrylamide with comonomers to prepare monodisperse hydrogel microspheres. Polym J 23:955–962
75. Martinez VS, Alvarez LP, Hernaez E, Herrero T, Katime I (2007) Synthesis, characterization, and influence of synthesis parameters on particle sizes of a new microgel family. J Polym Sci Polym Chem 45:3833–3842
76. Hazot P, Chapel JP, Pichot C, Elaissari A, Delair T (2002) Preparation of poly(N-ethyl methacrylamide) particles via an emulsion/precipitation process: the role of the crosslinker. J Polym Sci Polym Chem 40:1808–1817
77. Diaz-Camacho F, Lopez-Morales S, Vivaldo-Lima E, Saldivar-Guerra E, Vera-Graziano R, Alexandrova L (2004) Effect of regime of addition of initiator on TEMPO-mediated polymerization of styrene. Polym Bull 52:339–347
78. Downey JS, McIsaac G, Frank RS, Stöver DH (2001) Poly (divinylbenzene) microspheres as an intermediate morphology between microgel, macrogel, and coagulum in cross-linking precipitation polymerization. Macromolecules 34:4534–4541
79. Kolthoff IM, Miller IK (1951) The chemistry of persulfate. I. The kinetics and mechanism of decomposition of the persulfate ion in aqueous medium. J Am Chem Soc 73:3055–3059
80. Wu X, Pelton RH, Hamielec AE, Woods DR, McPhee W (1994) The kinetics of poly(N-isopropylacrylamide) microgel latex formation. Colloid Polym Sci 272:467–477
81. Duracher D, Elaissari A, Pichot C (1999) Preparation of poly(N-isopropylmethacrylamide) latexes: kinetic studies and characterization. J Polym Sci Polym Chem 37:1823–1837
82. Snowden MJ, Chowdhry BZ, Vincent B, Morris GE (1996) Colloidal copolymer microgels of N-isopropylacrylamide and acrylic acid: pH, ionic strength and temperature effects. J Chem Soc Faraday Trans 92:5013–5016